Dynamic large deformation analysis of a cantilever beam

H. Wei[1], Q.X. Pan[1], O.B. Adetoro[2], E. Avital[3], Y. Yuan[3], P.H. Wen[3*]

[1]*School of Traffic and Transportation Engineering, Changsha University of Science and Technology, China*
[2]*College of Engineering, Design and Physical Sciences, Brunel University, London UB8 3PH, UK*
[3]*School of Engineering and Materials Science, Queen Mary, University of London, London E1 4NS, UK*

Abstract

A static and dynamic large deformation analysis of a tapered beam subjected to concentrated and distributed loads is presented in this paper by using a direct integration technique. The bending stiffness of the beam is coordinate dependent. The nonlinear differential equation is numerically solved using an iterative technique without an algebraic equation solver, thus the computational effort can be reduced. A concentrated mass fixed at the free end and suddenly released is studied, and the time-dependent displacements are presented. Comparison has been made with solutions obtained using Finite Element Analysis and excellent agreement is achieved.

Key words: Nonlinear ordinary differential equation, large deformations, follower force, tapered beams, finite integration method, static and dynamic loads.

*Corresponding: p.h.wen@qmul.ac.uk (P.H.Wen)

1. Introduction

It is well-known that in the traditional beam bending theories, including thin and moderate thick beams, the geometric nonlinearity is generally ignored. In the early study of the geometric nonlinearity in the Euler–Bernoulli beam theory, analytical solutions for a uniform cross-section and a concentrated force at the free end were derived by Bisshop and Drucker [1]. Numerical schemes were proposed by Saxena and Kramer [2] for non-linear differential equations with concentrated force and moment at the beam's free end. Using elliptic integrals, the large deflection of the fluid-saturated poroelastic beams which are permeable in the axial direction and impermeable in the transverse directions were studied by Li et al. [3]. Seide [4], Chucheepsakul et al. [5] and Chucheepsakul et al. [6] studied the large deflection of Euler-Bernoulli beam due to geometric nonlinearity with simply supported conditions subjected to a moment at the end. The shooting optimization technique was applied to deal with a simply supported beam under both concentrated and uniformly distributed forces by Wang and Kitipornchai [7]. Kimball and Tsai [8] solved the large deflection problem under combined end loadings using elliptic integrals and differential geometry. More recently, Wang et al [9] applied the homotogy analysis method for the large deformation of a cantilever beam under a point load at the free tip with the explicit analytic formulas in terms of rotation angle at the free tip, which provided a convenient and straightforward approach to calculate the vertical and horizontal displacements of the cantilever beam with large deformation.

The influence of shear deformation and frictional end supports were introduced in the large deformation of Timoshenko beam analysis by Li et al [10] and Peng et al [11]. Multiple equilibrium solutions of the uniform cantilever under a dead load were derived by Batista and Kosel [12]. The solution of large deflections of a beam under three-point-bending in terms of Jacobi elliptical functions was obtained by Batista [13]. Argyris and Symeonidis [14] studied static nonlinear analysis of a cantilever beam subjected to follower loads by the finite element method in order to find the critical flutter loads. A direct method for the large deflection problem of a non-uniform spring-hinged cantilever beam under a tip follower force was proposed by Shvartsman [15].

In the optimization of structures aimed at reducing structure weight, the design with a variable cross-section and functionally graded material has been introduced in engineering. However, it is difficult to obtain analytical solutions due to the complexity of the differential

equation. The most efficient way is the finite element analysis. Wood and Zienkiewicz [16] studied the large deformation of a non-uniform column subjected to an eccentric axial compressive force in the early years. A weight residual method was proposed by Baker [17] and different numerical approaches by Lee et al. [18], Nguyen and Buntara [19], Banerjee et al [20] and Saje [21]. Rao et al. [22,23,24] investigated large deflections for uniform/non-uniform cantilever beams subjected to a moment at the tip using the elliptic-function and the shooting method.

It has been shown that the finite integration method (FIM) proposed recently by Wen et al. [25] is one of the most accurate and efficient methods to solve partial differential equations. It has been extended to nonlocal elasticity [26] and multi-dimensions in engineering [27]. Yun et al [28], Li et al. [29] and Li and Hon [30] have demonstrated the applications of FIM to solve stiff PDEs problems with its unconditional stability and distinct advantage in smoothing stiffness in terms of singularities, discontinuities and stiff boundary layers. Recently, Huang et al. [31] investigated static large deformation under a dead concentrated vertical or horizontal force with very extremely high accuracy by FIM. Based on the work [31], FIM is extended to the static/dynamic large deformation of a beam subjected to different kinds of load with the integration matrix by Trapezoidal rule in this paper. Brief introduction of the finite integration method is given with a Lagrange series interpolation in Section 2. Analytical study and application of FIM to the large deformation of the beam under follower concentrated forces are given in Section 3. In section 4, the observation of a follower distributed force and the pressure load is presented. A concentrated mass fixed at the free tip that is suddenly released is studied in Chapter 5. Several examples are presented for a cantilever beam with constant or variable bending stiffness under different loads and dynamic case to demonstrate the applicability of FIM.

2. Finite integration method for one dimension statics

The concept of the integration matrix was proposed firstly by Wen et al [25] and the first-order integration matrix was directly obtained by integration with Trapezoidal rule, Simpson rules, Cotes formula and Lagrange formula. By observing the applications in different areas of science and engineering, we notice that the Lagrange formula provides the highest accurate

results for static cases. By Lagrange interpolation, the function $u(x)$ is approximated, in terms of the nodal values, as

$$u(x)=\sum_{j=1}^{N}\prod_{\substack{k=1\\k\neq j}}^{N}\frac{(x-x_k)}{(x_j-x_k)}u_j,\quad 0\le x\le 1 \tag{1}$$

where u_j denotes the nodal value at node j. For the uniformly distributed node in the region, we have

$$x_i=(i-1)/(N-1),\quad i=1,2,...,N, \tag{2}$$

where N denotes the number of nodes. For the non-uniformly distributed node, we preferably select the node coordinate as

$$x_i=\frac{1}{2}\left[1-\cos\frac{\pi(i-1)}{N-1}\right],\quad i=1,2,...,N. \tag{3}$$

For the sake of convenience, Lagrange interpolation can be written, in terms of a polynomial, as following

$$u(x)=\sum_{k=1}^{N}c_k x^{k-1}\ , \tag{4}$$

where the coefficient vector $\{c_k\}_{k=1}^{N}$ can be determined by nodal values of the function $u(x)$

$$\mathbf{c}=\mathbf{B}^{-1}\mathbf{u}, \tag{5}$$

in which the matrix and vectors are defined as

$$\mathbf{B}=\begin{pmatrix}1 & x_1 & x_1^2 & ... & x_1^{N-1}\\ 1 & x_2 & x_2^2 & ... & x_2^{N-1}\\ ... & ... & ... & ... & ...\\ 1 & x_N & x_N^2 & ... & x_N^{N-1}\end{pmatrix},\ \mathbf{c}=\begin{pmatrix}c_1\\ c_2\\ ...\\ c_N\end{pmatrix},\ \mathbf{u}=\begin{pmatrix}u_1\\ u_2\\ ...\\ u_N\end{pmatrix}. \tag{6}$$

Carrying out integration over both sides of Eq.(4) in the region of $[0,x_i]$, we obtain

$$U(x_i)=\int_0^{x_i}u(x)dx=\sum_{k=1}^{N}\frac{c_k}{k}x_i^k,\quad i=1,2,...,N. \tag{7}$$

Considering the vector of the coefficient in (5), we obtain the nodal values of integration $U(x_i)$ from Eq.(7) in matrix form

$$\mathbf{U} = \tilde{\mathbf{A}}\mathbf{c} = \tilde{\mathbf{A}}\mathbf{B}^{-1}\mathbf{u} = \mathbf{A}\mathbf{u} \tag{8}$$

where $U = \{U_i, U_2, ..., U_N\}^T$ and matrix

$$\tilde{\mathbf{A}} = \begin{pmatrix} x_1 & x_1^2/2 & x_1^3/3 & ... & x_1^N/N \\ x_2 & x_2^2/2 & x_2^3/3 & ... & x_2^N/N \\ ... & ... & ... & ... & ... \\ x_N & x_N^2/2 & x_N^3/3 & ... & x_N^N/N \end{pmatrix}. \tag{9}$$

Extending the first integration concept to a multi-layer integration, we obtain

$$U^{(2)}(x) = \int_0^x \int_0^x u(\xi) d\xi dx, \qquad x \in [0, a]. \tag{10}$$

From expression Eq.(7), we obtain double-later integrals

$$U^{(2)}(x_i) = \sum_{k=1}^{N} \frac{c_k}{k(k+1)} x_i^{(k+1)}, \quad i = 1,2,..., N. \tag{11}$$

Considering the coefficient vector in Eq.(5), we obtain the nodal values of the double-layer integration

$$\mathbf{U}^{(2)} = \tilde{\tilde{\mathbf{A}}}\mathbf{c} = \tilde{\tilde{\mathbf{A}}}\mathbf{B}^{-1}\mathbf{u} = \mathbf{A}^{(2)}\mathbf{u}, \tag{12}$$

where

$$\tilde{\tilde{\mathbf{A}}} = \begin{pmatrix} x_1^2/2 & x_1^3/6 & x_1^4/12 & ... & x_1^{N+1}/N/(N+1) \\ x_2^2/2 & x_2^3/6 & x_2^4/12 & ... & x_2^{N+1}/N/(N+1) \\ ... & ... & ... & ... & ... \\ x_N^2/2 & x_N^3/6 & x_N^4/12 & ... & x_N^{N+1}/N/(N+1) \end{pmatrix}. \tag{13}$$

This integration matrix can be easily extended to multi-layer integrals which are defined as

$$U^{(m)}(x) = \int_0^x ... \int_0^z u(y) dy ... dx, \qquad y, z, ... x \in [0, a] \tag{14}$$

For *m*-th multi-layer integration of function $u(x)$ at each node, we obtain the nodal integration value in matrix form, approximately, by

$$\mathbf{U}^{(m)} = \mathbf{A}^{(m)}\mathbf{u} \cong \mathbf{A}^m\mathbf{u} \tag{15}$$

The applications of FIM in elasticity and heat transformation can be found in [12,13].

3. Analysis for concentrated follower forces

3.*1 Analytical solution under a concentrated force and moment.*

Consider a cantilever beam with a constant bending stiffness subjected to a concentrated follower concentrated force P and moment M at the end shown in Figure 1. By Euler–Bernoulli beam theory, the curvature of the beam gives

$$\frac{d\theta}{ds'} = \frac{P}{EI}\left[\cos(\beta\theta_B)\left(x'_B - x'\right) + \sin(\beta\theta_B)\left(w'_B - w'\right)\right] + \frac{M}{EI},\ \theta\big|_{s=0} = 0,\ 0 \le \beta \le 1,\ 0 \le x' \le x'_B \quad (16)$$

where θ denotes the rotation or slop of the beam, s' is the natural distance measured from the fixed end, θ_B is the rotation at the free end, and β represents a dimensionless factor. If β is zero, it means that the concentrated force is a dead load such as gravity. If $\beta = 1$, it corresponds to the follower force which is always perpendicular to the deformed beam at the end. Considering $dx'/ds' = \cos\theta$ and $dw'/ds' = \sin\theta$, we obtain the second-order derivative of the rotation from Eq.(16)

$$EI\frac{d^2\theta}{ds'^2} = -P\cos(\beta\theta_B - \theta),\ \ \theta\big|_{s=0} = 0,\ \ \left.\frac{d\theta}{ds'}\right|_{s=L} = M/EI \quad (17)$$

Introducing new dimensionless notations

$$\alpha = \frac{PL^2}{EI},\ m = \frac{ML}{EI},\ x = \frac{x'}{L}, w = \frac{w'}{L} \text{ and } s = \frac{s'}{L} \quad (18)$$

expression (17) becomes

$$\left(\frac{d\theta}{ds}\right)^2 = 2\alpha[\sin(\beta\theta_B - \theta) - \sin(\beta - 1)\theta_B] + m^2,\ \ \theta\big|_{s=0} = 0,\ \ 0 \le s \le 1 \quad (19)$$

By one integration, we find

$$s = \frac{1}{\sqrt{2\alpha}}\int_0^{\theta} \frac{d\theta}{\sqrt{\sin(\beta\theta_B - \theta) - \sin(\beta - 1)\theta_B + m^2/2\alpha}}. \quad (20)$$

At the free end $(s = 1)$, we obtain

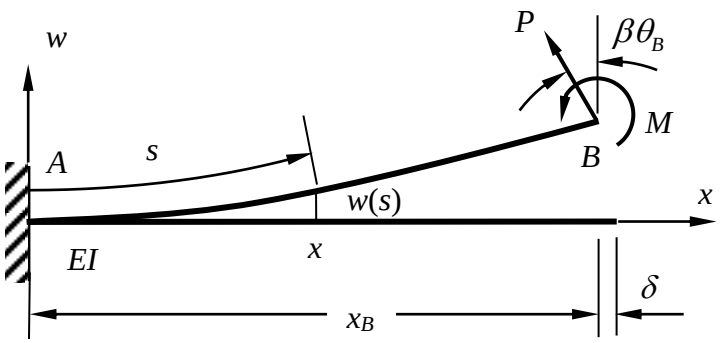

Figure 1. Cantilever beam in natural coordinate under concentrated forces at the end.

$$1=\frac{1}{\sqrt{2\alpha}}\int_0^{\theta_B}\frac{d\theta}{\sqrt{\sin(\beta\theta_B-\theta)-\sin(\beta-1)\theta_B+m^2/2\alpha}}\,. \tag{21}$$

For a dead load, i.e. $\beta=m=0$, expression (21) becomes

$$\sqrt{\alpha}=\sqrt{2\sin\theta_B}\int_0^{1}\frac{dt}{\sqrt{1-\sin^2\theta_B(1-t^2)^2}}\,. \tag{22}$$

For a follower force, $\beta=1,\ m=0$, we have

$$\sqrt{\alpha}=\frac{1}{\sqrt{2}}\int_0^{\theta_B}\frac{d\theta}{\sqrt{\sin(\theta-\theta_B)}} \tag{23}$$

By integrations, either analytically or numerically, we obtain the load factor α in terms of the rotation θ_B with elliptical functions [12]. In addition, two displacements of the beam are evaluated by

$$w(s)=\int_0^{s}\sin\theta ds\,,\ \ x(s)=\int_0^{s}\cos\theta ds\,, \tag{24}$$

and at the free end, we have

$$w_B=\frac{1}{\sqrt{2\alpha}}\int_0^{\theta_B}\frac{\sin\theta d\theta}{\sqrt{\sin(\beta\theta_B-\theta)-\sin(\beta-1)\theta_B+m^2/2\alpha}} \tag{25}$$

and

$$x_B = \frac{1}{\sqrt{2\alpha}} \int_0^{\theta_B} \frac{\cos\theta d\theta}{\sqrt{\sin(\beta\theta_B - \theta) - \sin(\beta - 1)\theta_B + m^2/2\alpha}}. \tag{26}$$

From Eq.(19), it can be seen that the following relations between rotations and load factors must hold

$$[\sin(\beta\theta_B - \theta) - \sin(\beta - 1)\theta_B] + m^2/2\alpha \geq 0. \tag{27}$$

If $m^2/2\alpha \geq 2$, Eq.(27) is always satisfied for any solutions of θ and θ_B. This requirement of rotation divides the entire plane (θ_B, θ) into a network of alternating positively and negatively signed regions. Seeing from Figure 2 to Figure 9, the regions in dark blue are those where a solution is not possible.

Let $\theta = 0$ in Eq.(27) in order to determine points *a* and *b* in those figures, we obtain

$$\sin\beta\theta_B - \sin(\beta - 1)\theta_B + m^2/2\alpha = 0 \tag{28}$$

Therefore, a series of roots collocated on the horizontal axis $\theta = 0$ such as points *a* and *b* in those figures can be determined. In order to determine the coordinate of points *c* and *d*, we rewrite rotation θ in terms of θ_B, from Eq.(27), as

$$\theta = \beta\theta_B - \arcsin[\sin(\beta - 1)\theta_B + m^2/2\alpha] \tag{29}$$

and then the horizontal coordinates corresponding to the points *c* and *d* are obtained respectively by

$$\theta_0 = \frac{1}{1-\beta}\arcsin\left(1 - \frac{m^2}{2\alpha}\right) \tag{30}$$

$$\theta_B^* = \begin{cases} \theta_0/(1-\beta) & \text{for point } d \\ -(\theta_0 + 1)/(1-\beta) & \text{for point } c \end{cases} \tag{31}$$

The vertical coordinates of rotation θ for those two points are determined

$$\theta^* = \beta\theta_B^* + \frac{\pi}{2} + 2k\pi \qquad k = 0, \pm 1, \pm 2, \ldots \tag{32}$$

Let us observe the solutions of rotation at free end θ_B/π in the region of $[-2,2]$. It is clear that the rotation θ must satisfy $\theta=\theta_B\,(s=1)$ and $\theta=0\,(s=0)$ at two ends of the beam. Three load environments are observed:

Case (1): $\beta=0$ (dead load), Figures 2, 3 and 4 show the domains of possible solution collocated in the plane (θ_B,θ) for different ratio of load factors m^2/α. Seeing from Eq.(32), as $\beta=0$, rotation angle θ at points *c* and *d* are independent of force factors *m* and α. It is obvious that the rotation angle at the end θ_B must locate in the regions of *Ca* and *bD* shown in those figures. It can also be seen from Figure 2 that in those regions the integration starts from $\theta=0$ in any direction between the points *E* and *F*, where we can reach the line $\theta_B=\theta$ (shown in thick dark line). The coordinates of those points are listed in Table 1.

Table 1. The locations of critical point for $\beta=0$.

Point	$m^2/2\alpha=0$		$m^2/2\alpha=0.5$		$m^2/2\alpha=1$	
	θ_B/π	θ/π	θ_B/π	θ/π	θ_B/π	θ/π
a	-1.0	0.0	-5/6	0.0	-0.5	0.0
b	0.0	0.0	-1/6	0.0	-0.5	0.0
c	-1.5	0.5	-7/6	0.5	-1.0	0.5
d	0.5	0.5	1/6	0.5	0.0	0.5
C	-1.5	0.0	-11/6	0.0	-2.0	0.0
D	0.5	0.0	5/6	0.0	1.0	0.0

Case (2): $\beta=0.5$, Figures 5, 6 and 7 show the domains of the possible solution in the plane (θ_B,θ) for different ratios of load factor m^2/α. When $m^2/\alpha=0$, the horizontal coordinates for points *C* and *a*, *b* and *D* are the same respectively. The solution of rotation θ_B has to be collocated in the regions of *Ca* and *bD*. The coordinates of those points are illustrated in Table 2 for different load ratios $m^2/2\alpha$.

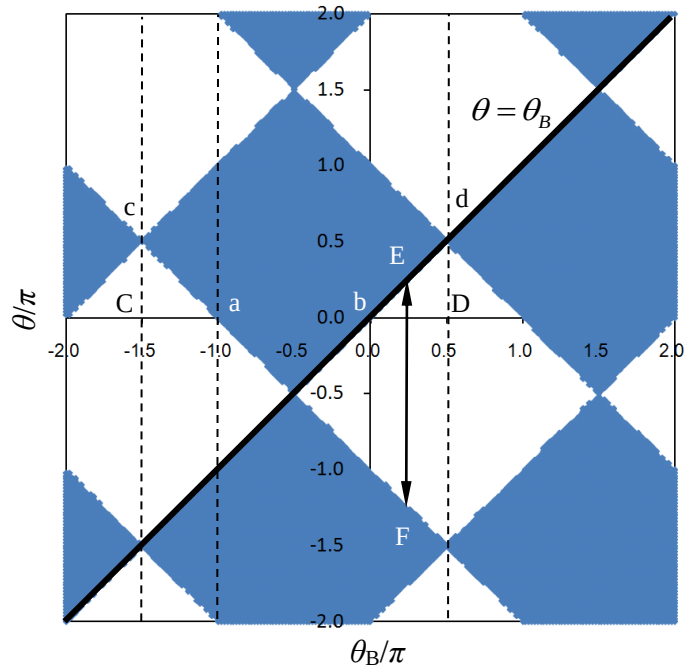

Figure 2. Domains of possible solutions for parameter $\beta = m = 0$.

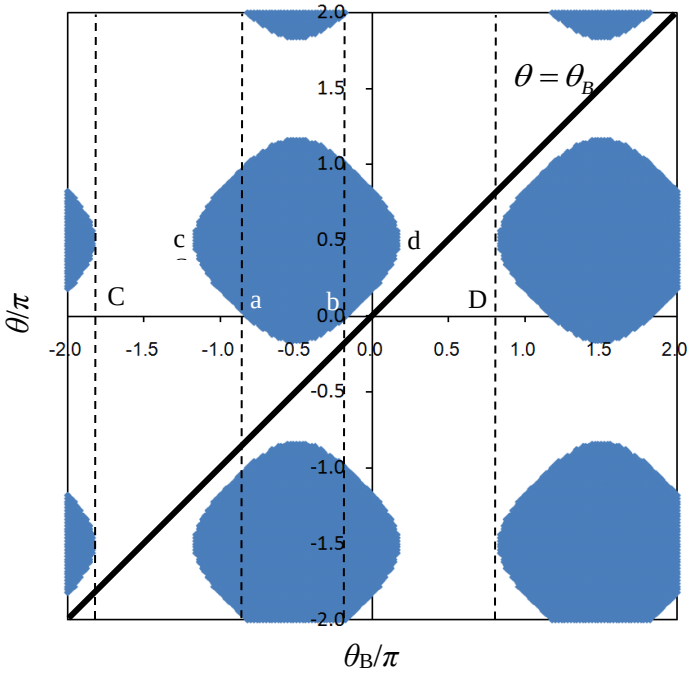

Figure 3. Domains of possible solutions for parameter $\beta = 0$ and $m^2 / 2\alpha = 0.5$

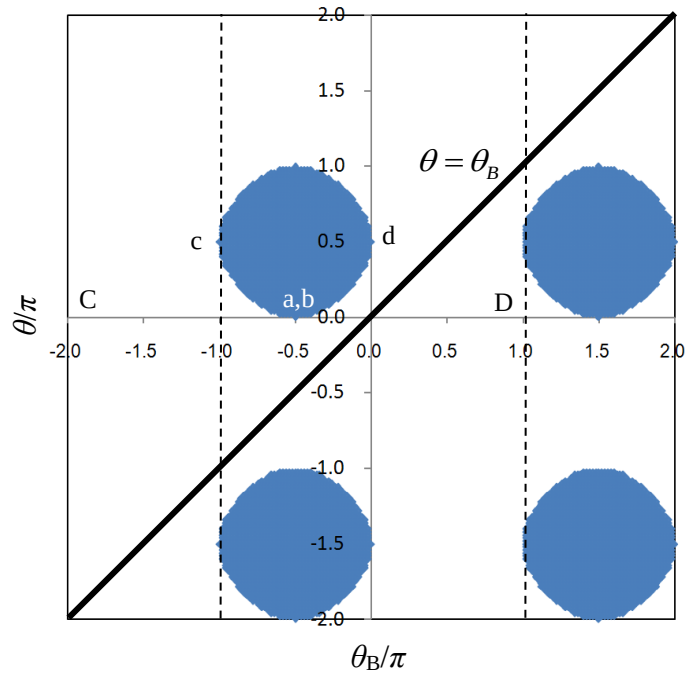

Figure 4. Domains of possible solutions for parameter $\beta = 0$ and $m^2 / 2\alpha = 1$

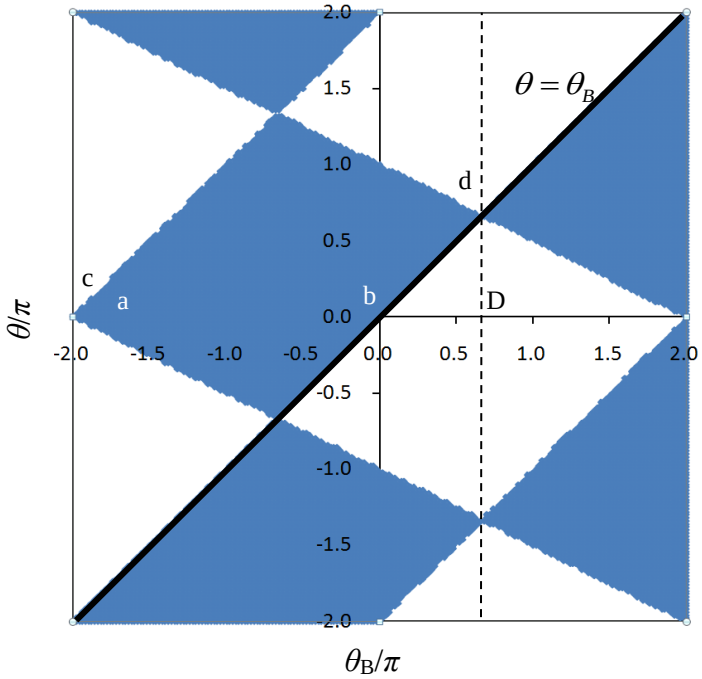

Figure 5. Domains of possible solutions for parameter $\beta = 0.25$ and $m = 0$

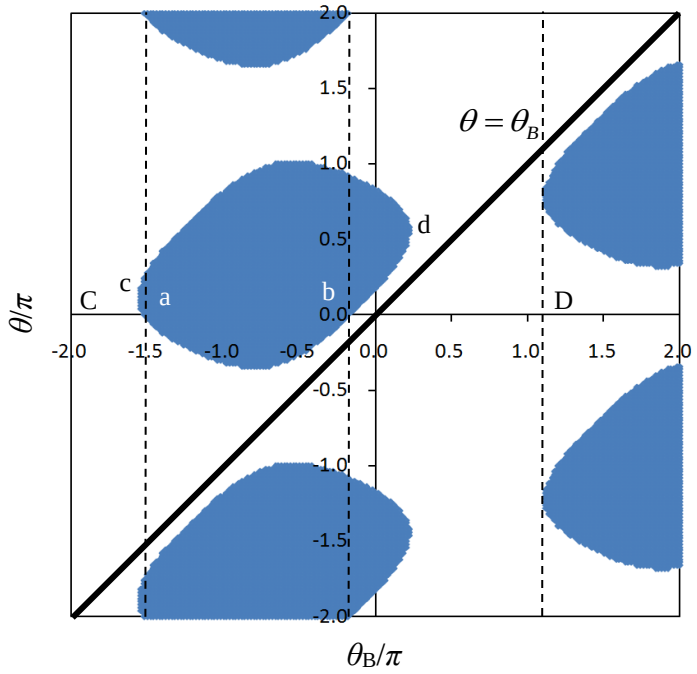

Figure 6. Domains of possible solutions for parameter $\beta = 0.25$ and $m^2/2\alpha = 0.5$.

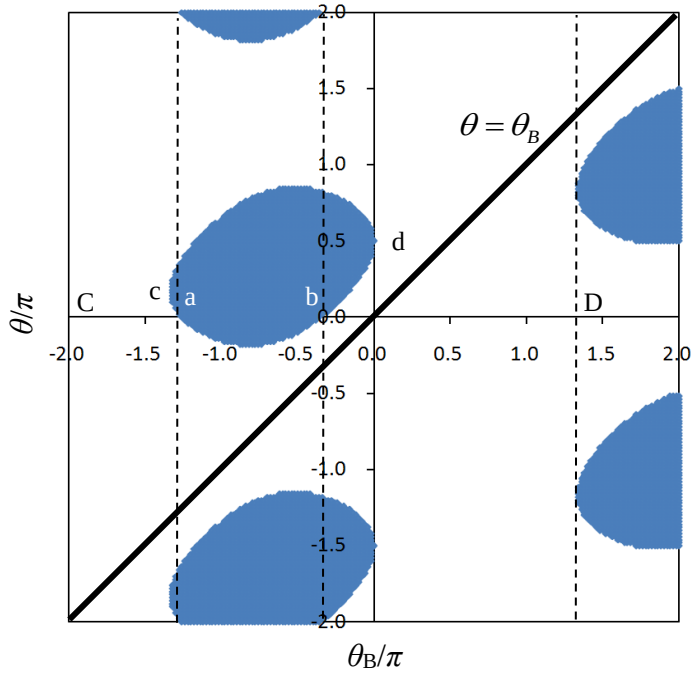

Figure 7. Domains of possible solutions for parameter $\beta = 0.25$ and $m^2/2\alpha = 1$.

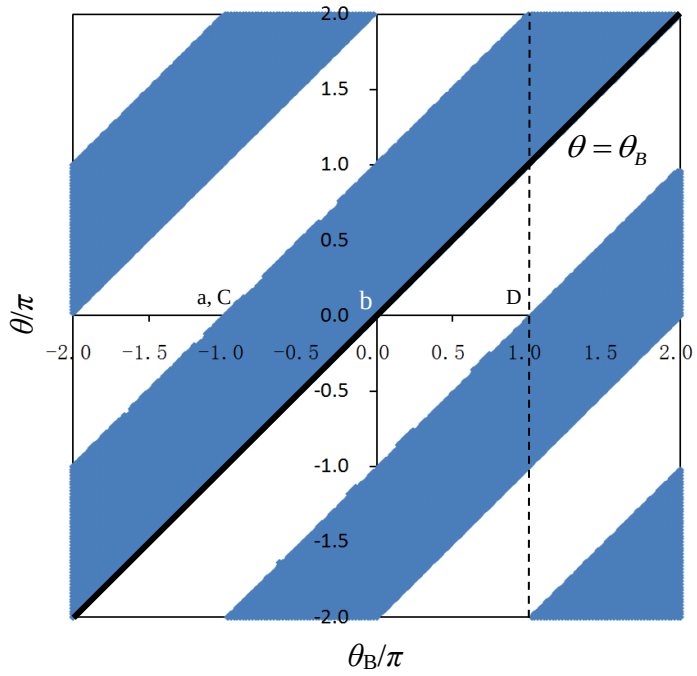

Figure 8. Domains of possible solutions for parameter $\beta = 1.0$ and $m = 0$

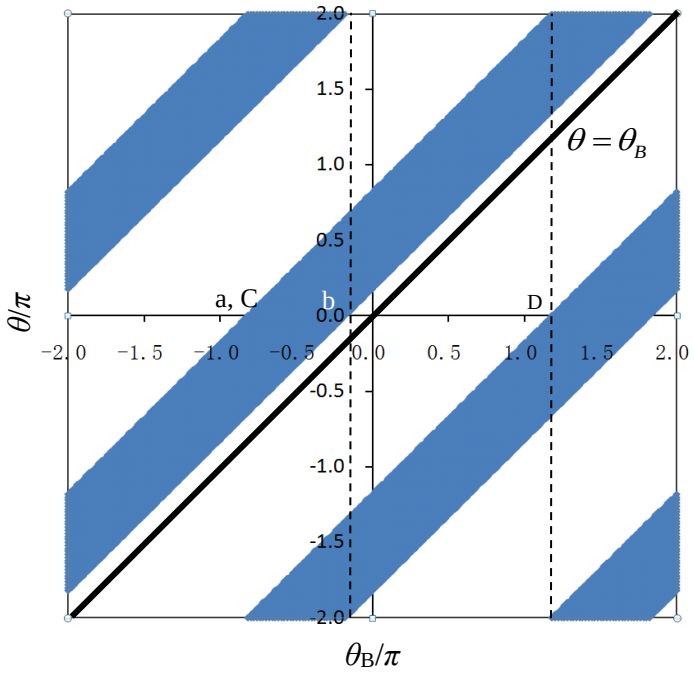

Figure 9. Domains of possible solutions for parameter $\beta = 1.0$ and $m^2 / 2\alpha = 0.5$.

Case (3): $\beta = 1$ (follower force), Figures 8 and 9 present the regions of solutions with different load factors at the end. The collocations of the negative region, in this case, become the roots of the following equation

$$\sin(\theta_B - \theta) + m^2 / 2\alpha = 0 \tag{33}$$

Table 2. The locations of critical point for $\beta = 1/4$.

Point	$m^2/2\alpha = 0$		$m^2/2\alpha = 0.5$		$m^2/2\alpha = 1$	
	θ_B/π	θ/π	θ_B/π	θ/π	θ_B/π	θ/π
a	-2.0	0.0	-1.524	0.0	-1.264	0.0
b	0.0	0.0	-1.6	0.0	-0.348	0.0
c	-2.0	0.0	-14/9	1/9	-4/3	1/6
d	2/3	2/3	2/9	5/9	0.0	0.5
C	-2.0	0.0	-2.0	0.0	2.0	0.0
D	2/3	0.0	10/9	0.0	4/3	0.0

All collocations of those critical points can be obtained easily. In this case, the regions of the realistic solution become a series of strip and region *Ca* disappears. Obviously, the strip of the negative region becomes narrow when the ratio of factor m^2/α increases. However, if $m^2/2\alpha \geq 1$, the negative regions disappear completely.

3.2 Numerical solution for uniform cross-section and tapered beams

Let us consider the finite integration method in order to solve the nonlinear differential equation (16) numerically. We have two options for the node distribution. The first option is the uniform distribution over the region [0,1] and the coordinates are specified as

$$s_i = (i-1)/(N-1), \quad i = 1,2,...,N, \tag{34}$$

where *N* denotes the number of nodes. The second option is the non-uniform distribution over the domain

$$s_i = \frac{1}{2}\left[1 - \cos\frac{\pi(i-1)}{N-1}\right], \quad i = 1,2,...,N. \tag{35}$$

The curvature of the beam bending in (16) is rewritten, in the normalized form, as

$$\frac{d\theta}{ds} = \alpha\left[\cos(\beta\theta_B)\left(x_B - x\right) + \sin(\beta\theta_B)\left(w_B - w\right)\right] + m,\ 0 \le \beta \le 1,\ 0 \le s \le 1\ . \tag{36}$$

Considering a cantilever non-uniform cross-section beam using FIM with the integration matrix in Eq.(8), we obtain

$$\boldsymbol{\theta} = \mathbf{A}\mathbf{h} \tag{37}$$

in which

$$\mathbf{h} = \left\{h_1, h_{2,\ldots,} h_N\right\}^T,\quad h_i = \alpha_i\left[\cos(\beta\theta_B^{(p)})\left(x_B^{(p)} - x_i^{(p)}\right) + \sin(\beta\theta_B^{(p)})\left(w_B^{(p)} - w_i^{(p)}\right)\right] + m_i,$$

$$\alpha_i = \frac{Pl^2}{EI(s_i)} \text{ and } m_i = \frac{Ml}{EI(s_i)}. \tag{38}$$

where subscript *p* denotes the number of the iterative step. Applying the iterative technique, we obtain the nodal rotations at each step and the vectors of deformation from Eq.(36)

$$\mathbf{w} = \mathbf{A}\mathbf{f}_s \text{ and } \mathbf{x} = \mathbf{A}\mathbf{f}_c \tag{39}$$

in which $\mathbf{f}_s = \left\{\sin\theta_i\right\}^{\mathrm{T}}$ and $\mathbf{f}_c = \left\{\cos\theta_i\right\}^{\mathrm{T}}$. Therefore, we obtain the numerical solutions by the following steps:

Step 1: Set $p = 0$ and initial rotation $\boldsymbol{\theta}^{(0)} = \mathbf{0}$;

Step 2: Calculate vectors $\mathbf{h}^{(p)}$, $\mathbf{f}_s^{(p)}$ and $\mathbf{f}_c^{(p)}$;

Step 3: Determine the rotations for current step using integration matrix

$$\boldsymbol{\theta}^{(p+1)} = \mathbf{A}\mathbf{h}^{(p)} \tag{40}$$

Step 4: Calculate displacements $\mathbf{w}^{(p+1)}$ and $\mathbf{x}^{(p+1)}$ from (34)

Step 5: Check the relative error at free end

$$\eta = \frac{\left|w_B^{(p+1)} - w_B^{(p)}\right|}{w_B^{(p)}}, \text{ if } \eta < 10^{-5} \text{ go to Step 8;} \tag{41}$$

Step 6: Modify rotation for next step

$$\boldsymbol{\theta}^{(p+1)} = \lambda\boldsymbol{\theta}^{(p)} + (1-\lambda)\boldsymbol{\theta}^{(p+1)}, \tag{42}$$

Step 7: set $p = p + 1$ and go to Step 2;`

Step 8: Print results and Stop.

In addition, the computation procedure is demonstrated in the flowchart in Figure 10.

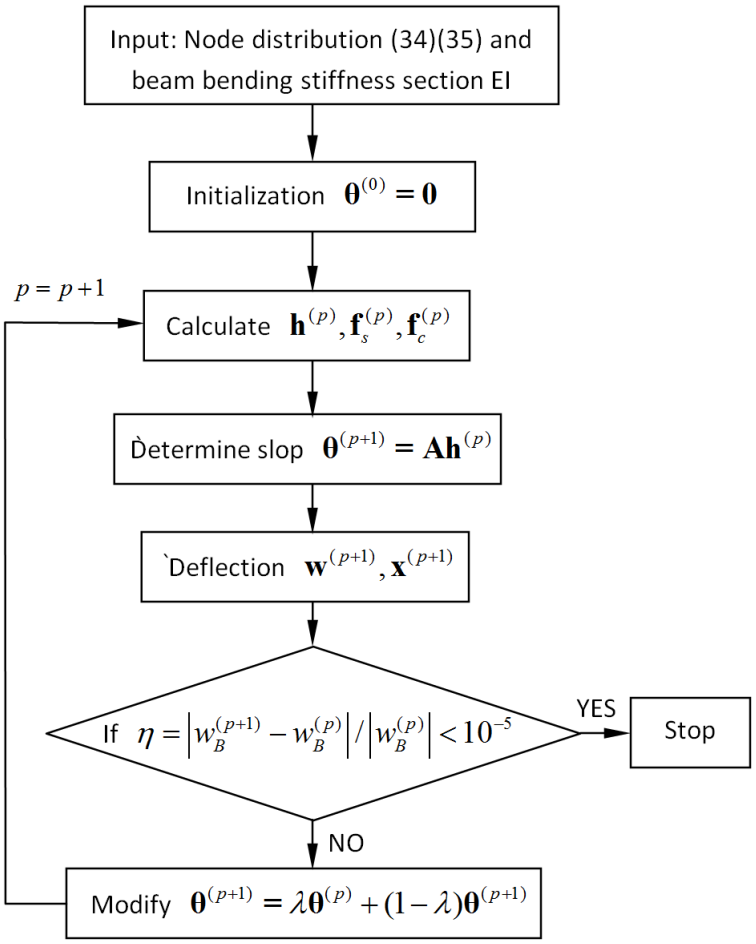

Figure 10. Computation iterative steps for nonlinear problem.

Let us begin with a uniform cross-section beam subjected to a concentrated force only at the free end. Non-uniformly distributed nodes are considered and the node number in total is $N = 11$. Figures 11(a)(b) and (c) present the deformation of the cantilever beam in the cases of $4 \le \alpha \le 14$, $16 \le \alpha \le 50$ and $52 \le \alpha \le 120$, respectively while the speed factor is $\lambda = 0.8$. In the case of $\alpha \le 13.75$, the analytical solutions [12,13] correspond to the first equilibrium configuration of the beam. In the region of $13.75 \le \alpha \le 55.0$, the results correspond to the second equilibrium configuration. We find three equilibrium configurations from Figures

10(a)(b) and (c) precisely. Obviously, the rotations satisfy $0 \le \theta_B \le \pi$ and $0 \le \theta \le \pi$ and these have been demonstrated in Figure 8.

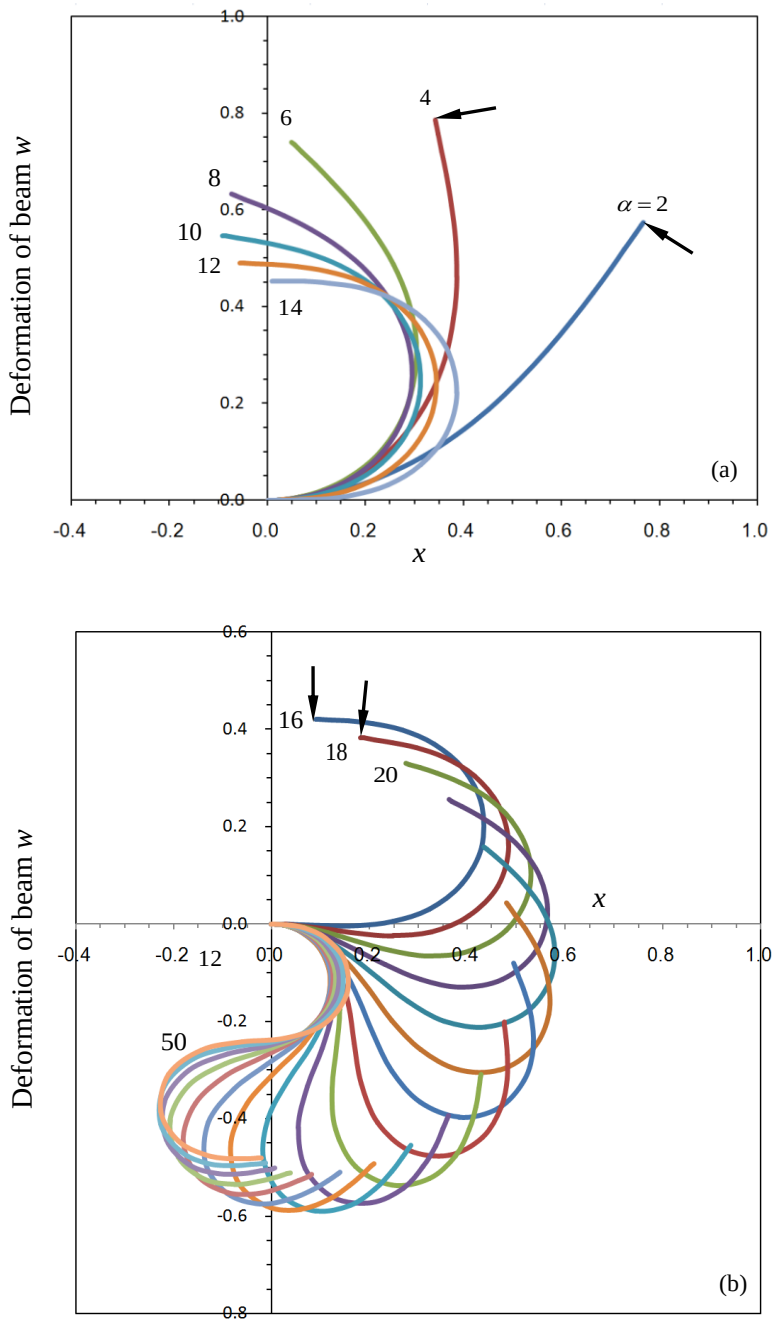

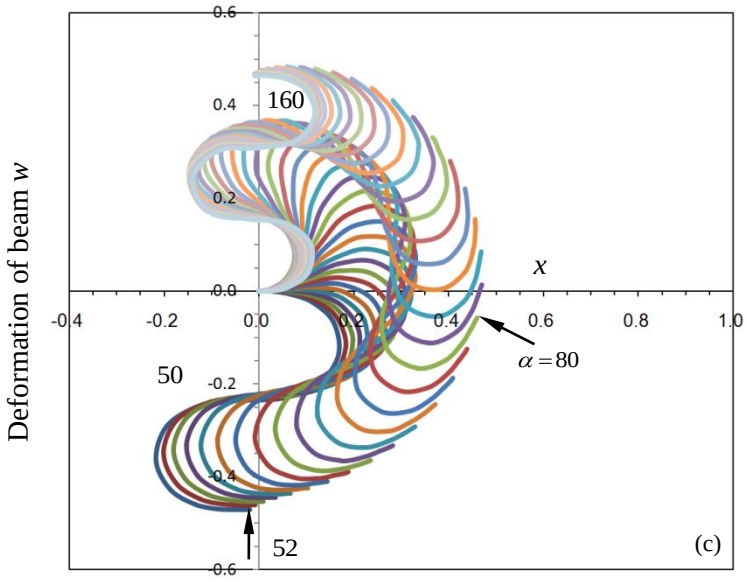

Figure 11. Deflection at the end w_B against normalized transverse force α.

We notice that the number of iteration circle is less than 20 in each case without algebraic equations being solved in the computational procedure. It means that the computational effort is reduced even for a nonlinear problem. Compared with the numerical solutions by Mutyalarrao et al [32] and Batisata [33], excellent agreement is achieved.

Secondly, we consider a tapered cross-section beam shown in Figure 12(a). The thickness of such a beam is usually a function of the nature coordinate *s* while the width is kept constant. The bending stiffness is defined as

$$EI(s) = (2-s)^3 EI_B, \quad EI_A = 8EI_B. \tag{43}$$

In this case, non-uniformly distributed nodes ($N = 19$) are applied as expressed in Eq.(10) along with $m = 0$ and speed factor $\lambda = 0.8$. The deformed configurations of the cantilever beam are shown in Figure 13 for $\alpha \le 80$ versus the load factor α. Numerical results show that the rotation at the end satisfies $\theta_B < \pi$ in all situations and the deformed tapered beams are located in the first and the fourth quadrants, i.e. $x(s) \ge 0$. The first and the second equilibrium deformations are observed easily in those curves. Changing the fixed/free ends with same geometry of the beam shown in Figure 12(b), we have bending stiffness

$$EI(s) = (1+s)^3 EI_B/8, \quad EI_A = EI_B/8. \tag{44}$$

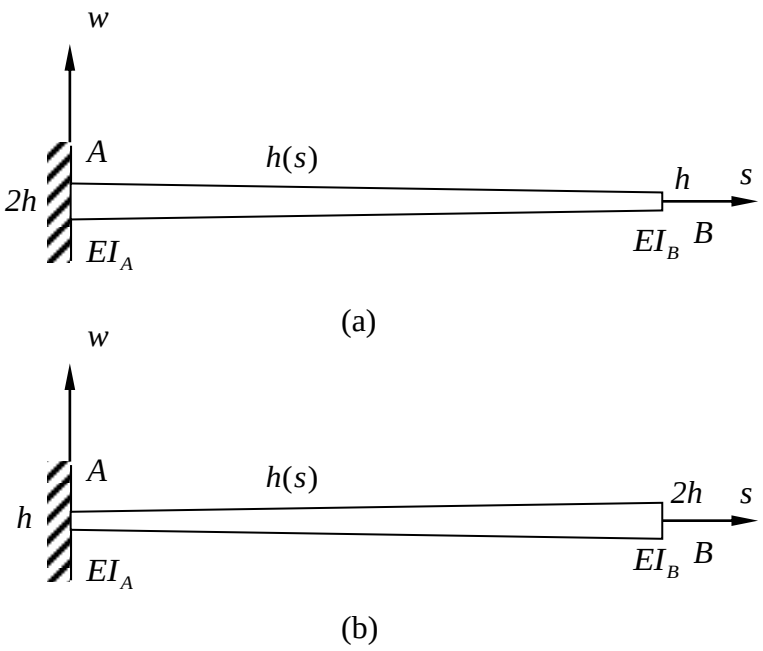

Figure 12. Variation of height against the natural coordinate.

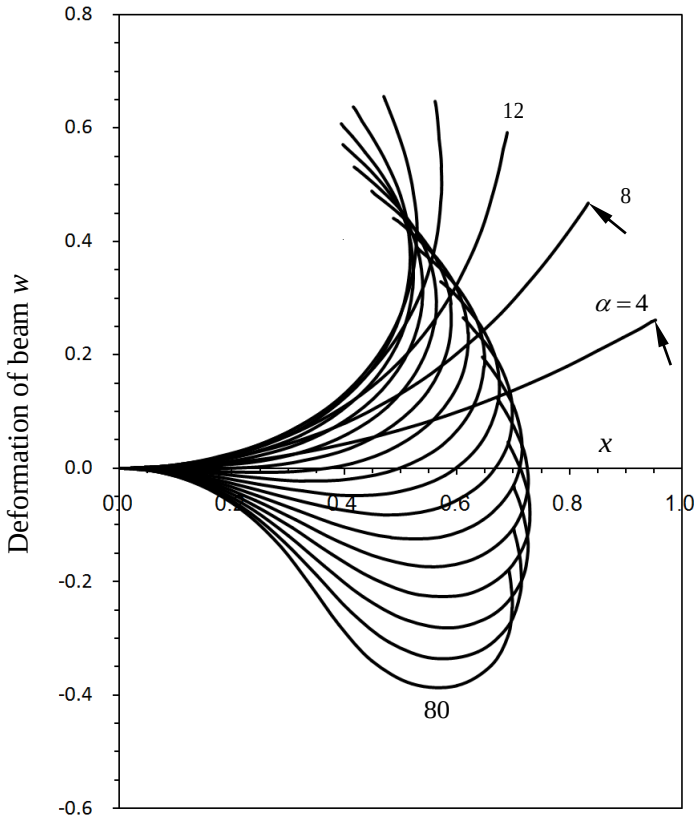

Figure 13. Deformation of beam under transverse force versus the transverse load factor α .

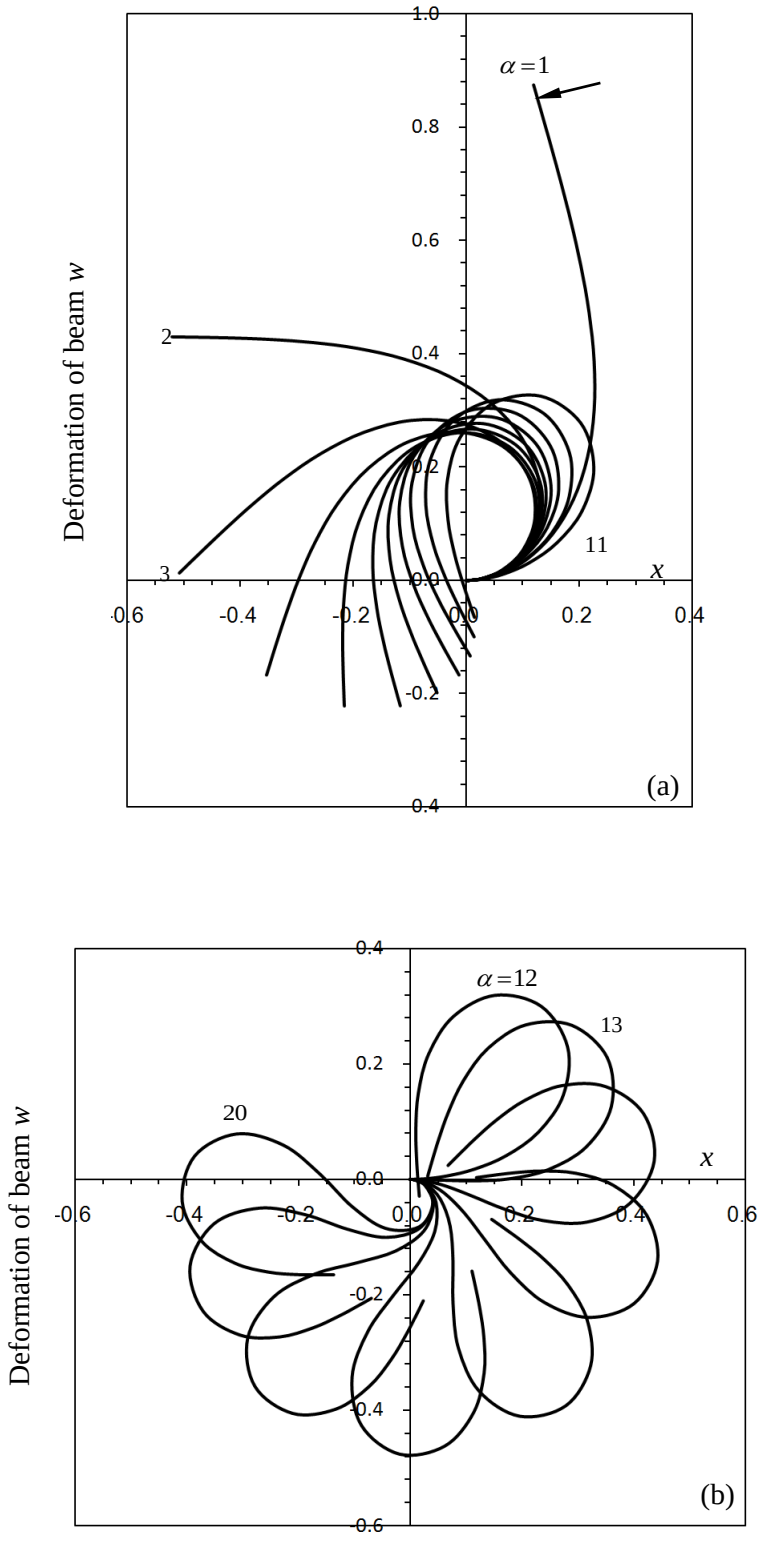

Figure 14. Deformation of beam under transverse force versus the transverse load factor α .

Using the same parameters in the previous example, we present the deformation curves of the tapered beam in Figure 14(a) for $1 \le \alpha \le 11$ and Figure 14(b) for $12 \le \alpha \le 20$, with the first and second equilibrium configurations, respectively.

4. Tapered beam under the constant follower distributed load

A cantilever beam is subjected to a uniformly distributed load of the intensity q_0 as shown in Figure 15. From classical Euler–Bernoulli beam theory, we obtain the equation of curvature

$$\frac{d\theta}{ds} = \frac{q_0}{EI(s)} \int_s^1 \left[(w(\xi) - w(s)) \sin\theta + (x(\xi) - x(s)) \cos\theta \right] d\xi \tag{45}$$

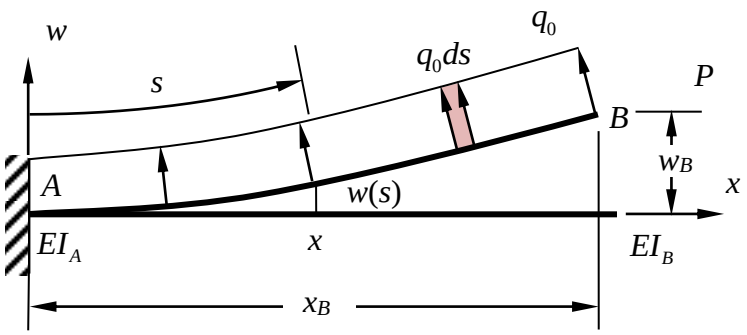

Figure 15. Cantilever beam subjected to a uniformly distributed load q_0.

Considering expression (24), we obtain

$$\begin{aligned} \frac{d\theta}{ds} &= \frac{q_0}{EI(s)} \int_s^1 \left[w(\xi) \sin\theta + x(\xi) \cos\theta \right] d\xi - \frac{q_0}{EI(s)} w(s) \left[w_B - w(s) \right] - \frac{q_0}{EI(s)} x(s) \left[x_B - x(s) \right] \\ &= h(x, w, \theta, s) \end{aligned} \tag{46}$$

Applying the integration matrix in FIM over the two sides of Eq.(46) with the boundary condition, we have

$$\boldsymbol{\theta} = \mathbf{A}\mathbf{h}, \quad . \tag{47}$$

in which

$$h_i(s_i) = \frac{q_0}{EI(s_i)} \int_{s_i}^{1} [w(\xi)\sin\theta + x(\xi)\cos\theta] d\xi - \frac{q_0}{EI(s_i)} w(s_i)[w_B - w(s_i)] - \frac{q_0}{EI(s_i)} x(s_i)[x_B - x(s_i)]. \tag{48}$$

To evaluate the definite integral in (47), we apply the integration matrix directly

$$\int_{s_i}^{1} [w(\xi)\sin\theta + x(\xi)\cos\theta] d\xi = \sum_{k=1}^{N} (A_{Nk} - A_{ik}) g_k \tag{49}$$

where $g_k = w(s_k)\sin\theta_k + x(s_k)\cos\theta_k$, $w(s_i)$ and $x(s_i)$ are the vertical and horizontal nodal displacements in Eq.(24). By using the same iterative algorithm as above, we find solutions for a tapered beam which carries a uniformly distributed load of density q_0 as follows:

Step 1: Set $p = 0$ and specify the initial rotation $\boldsymbol{\theta}^{(0)}$ as zero;

Step 2: Calculate vectors $\mathbf{f}_s^{(p)}$, $\mathbf{f}_c^{(p)}$ and then $\mathbf{h}^{(p)}$ from (48)

Step 3: Calculate nodal values of rotations

$$\boldsymbol{\theta}^{(p+1)} = \mathbf{A}\mathbf{h}^{(p)} \tag{50}$$

Step 4: Check the relative error of the deflection at the tip

$$\eta = \frac{\left| w_B^{p+1} - w_B^{p} \right|}{w_B^{p}} \qquad \text{if } \eta < 10^{-5} \text{ go to Step 7;} \tag{51}$$

Step 5: Introduce the speed up iterative factor λ and modify the deflection for the next iteration

$$\boldsymbol{\theta}^{(p+1)} = \lambda\boldsymbol{\theta}^{(p)} + (1-\lambda)\boldsymbol{\theta}^{(p+1)}, \tag{52}$$

Step 6: set $p = p+1$ and go to Step 2;

Step 7: Print results and terminate the computation.

Let us consider a cantilever beam with a constant bending stiffness EI_B subjected to a uniform distributed follower load. A uniform distribution of nodes expressed in (11) is selected and the nodes' number is $N = 19$ in total. The configurations of the beam are plotted in Figures 16(a) and (b) versus the load factor $\psi (= q_0 L^3 / EI_B)$ in the regions of $6 \le \psi \le 60$ and $66 \le \psi \le 114$ respectively, where the speed factor $\lambda = 0.8$. It can be seen from Figure 16(b) that the second equilibrium mode starts from $\psi = 114$. Finally we consider a tapered cantilever beam with bending stiffness shown in Eq.(43) and present the deformed curves in Figure 17 for

different force factors ψ in the case of $\psi \le 400$. By observing the numerical solutions of the deformation in Figure 17, we notice that there is only the first equilibrium configuration of the tapered beam under a distributed load of density q_0.

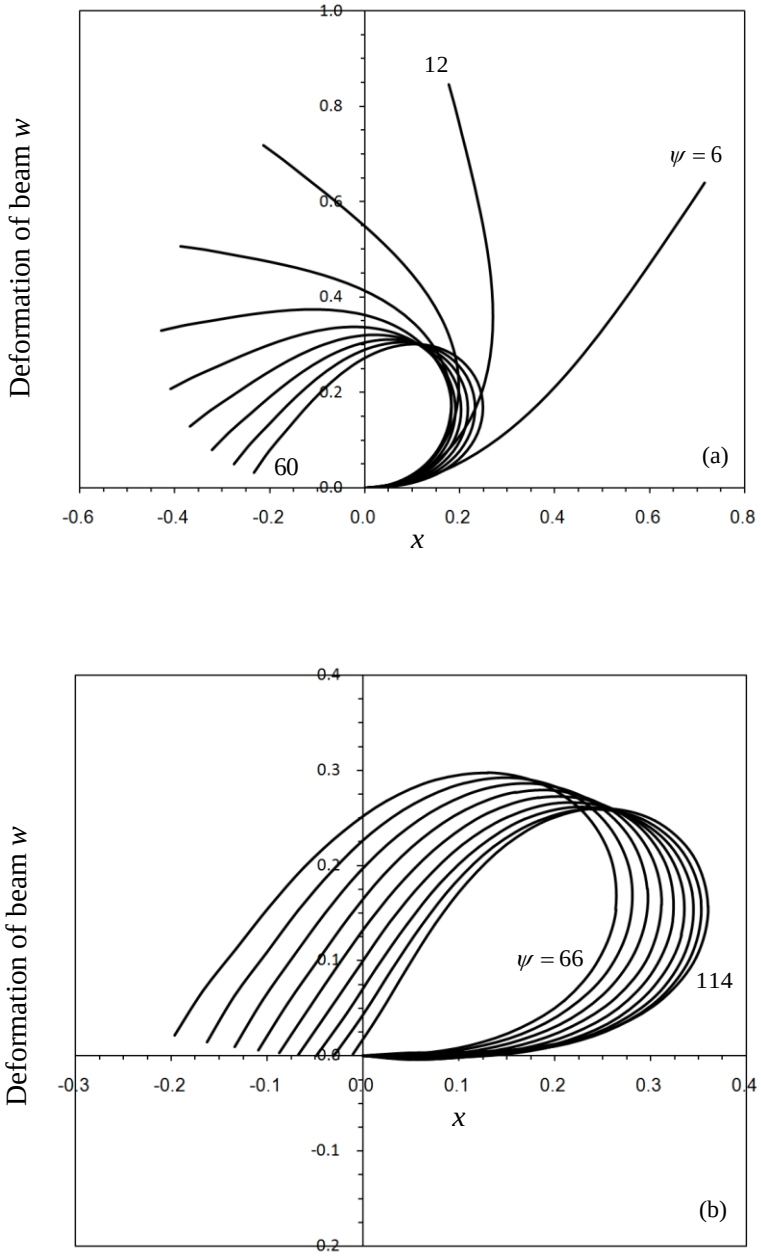

Figure 16. Deformation of beam under transverse force versus the transverse load α.

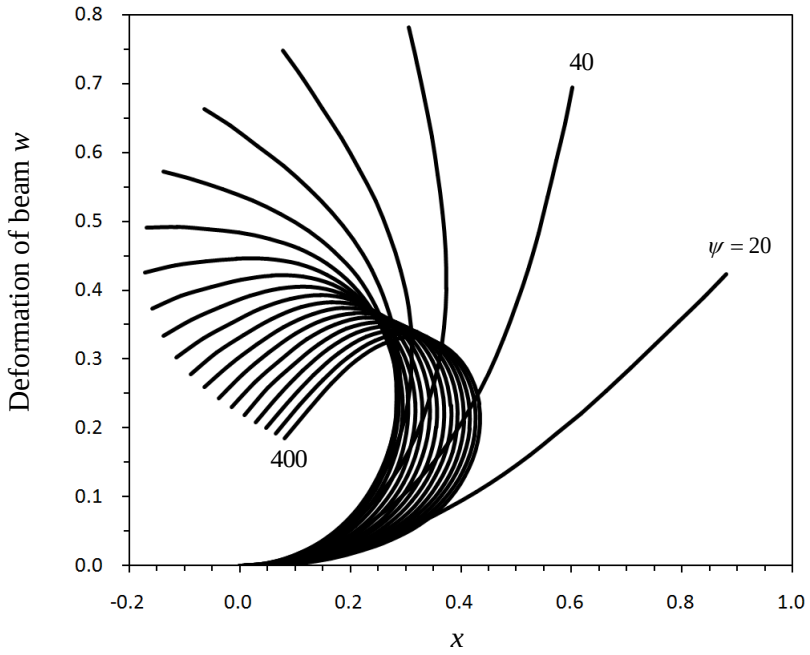

Figure 17. Deformation of beam under transverse force versus the transverse load α.

5. Cantilever beam with a concentrated mass at the free end

Consider a concentrated mass of *m* attached at the free end of the cantilever beam as shown in Figure 15 under the gravity force. The accelerations along horizontal and vertical directions are given by Newton's second law

$$m\frac{\partial^2 u_B}{\partial t^2} = -F_u(t),\ m\frac{\partial^2 w_B}{\partial t^2} = -mg - F_w(t),\ \ 0 \le t \le T \tag{53}$$

with initial conditions

$$u_B(0,x) = \frac{\partial u_B}{\partial t} = 0,\ w_B(0,x) = \frac{\partial w_B}{\partial t} = 0 \tag{54}$$

where T is the terminated value of time, F_u and F_w are reaction forces between concentrated mass and beam at the free end, and displacements satisfy

$$u_B = \int_0^1 \cos\theta ds - 1,\ w_B = \int_0^1 \sin\theta ds. \tag{55}$$

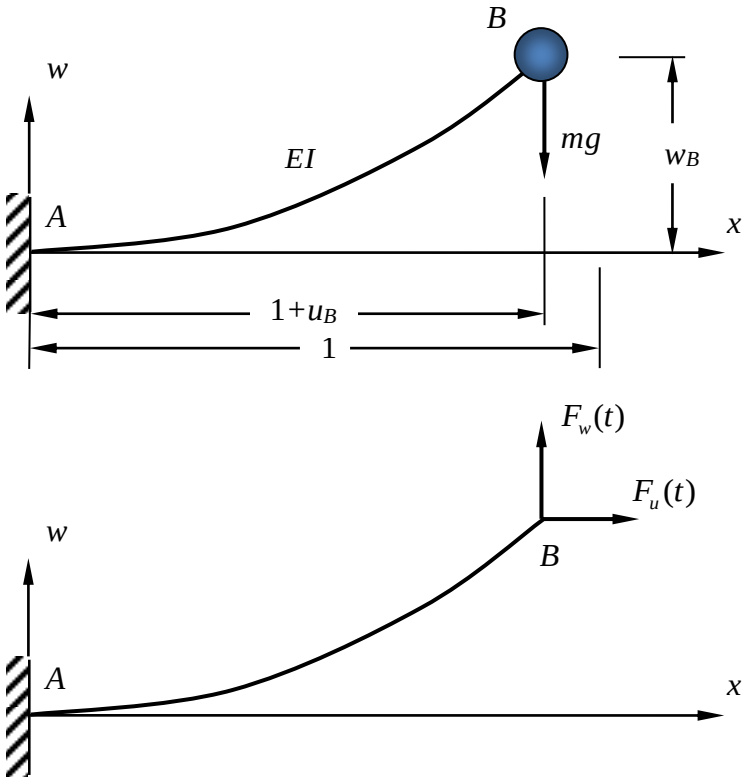

Figure 18. Large deformation of cantilever beam with concentrated mass.

By Euler–Bernoulli beam theory, the curvature of the beam gives

$$\frac{d\theta}{ds} = \frac{1}{EI}\left[F_w(t)\left(x_B - x\right) - F_u(t)\left(w_B - w\right)\right], \quad \theta\big|_{s=0} = 0, \;\; 0 \le x \le x_B \tag{56}$$

In the dynamic case, the first order integration matrix with Trapezoidal rule is more efficient and direct, which can be derived [21]

$$\mathbf{A}_t = (a_{ki}^{(1)}) = \begin{pmatrix} 0 & 0 & 0 & 0 & 0 & 0 \\ 1/2 & 1/2 & 0 & 0 & 0 & 0 \\ 1/2 & 1 & 1/2 & 0 & 0 & 0 \\ 1/2 & 1 & 1 & 1/2 & 0 & 0 \\ \cdots & \cdots & \cdots & \cdots & \cdots & \cdots \\ 1/2 & 1 & 1 & 1 & 1 & 1/2 \end{pmatrix} \Delta t \,. \tag{57}$$

where

$$a_{0i}^{(1)} = 0\,, \quad a_{ki}^{(1)} = \begin{cases} 0.5\Delta t & i = 0 \\ \Delta t & i = 1,2,...,k-1 \\ 0.5\Delta t & i = k \\ 0 & i > k \end{cases}, \quad \Delta t = T / N_t \tag{58}$$

where N_t is the number of time increment. The second order integration matrix gives

$$\mathbf{A}_t^{(2)} = (a_{ki}^{(2)}) = \mathbf{A}_t^2 = \begin{pmatrix} 0 & 0 & 0 & 0 & 0 & 0 \\ 1/4 & 1/4 & 0 & 0 & 0 & 0 \\ 3/4 & 1 & 1/4 & 0 & 0 & 0 \\ 5/4 & 2 & 1 & 1/4 & 0 & 0 \\ ... & ... & ... & ... & ... & ... \\ [1+2(N_t-2)]/4 & N_t-2 & N_t-3 & ... & 1 & 1/4 \end{pmatrix} (\Delta t)^2 \tag{59}$$

in which

$$a_{0i}^{(2)} = 0, \quad a_{ki}^{(2)} = \begin{cases} [1+2(k-2)](\Delta t)^2/4 & i = 0 \\ (k-i)(\Delta t)^2 & i = 1,2,...,k-1 \\ (\Delta t)^2/4 & i = k \\ 0 & i > k \end{cases} \tag{60}$$

Considering the initial conditions and applying integration matrix over two sides in Eq.(53) give

$$\mathbf{A}_t^2\mathbf{F}_u = \mathbf{I} - m\mathbf{u}_B,\ \mathbf{A}_t^2\mathbf{F}_w = -mg\mathbf{A}_t^2\mathbf{I} - m\mathbf{w}_B \tag{61}$$

where vectors

$$\mathbf{F}_u = \{F_u^1, F_u^2, ..., F_u^{N_t}\}^{\mathrm{T}}, \mathbf{F}_w = \{F_w^1, F_w^2, ..., F_w^{N_t}\}^{\mathrm{T}}, \mathbf{I} = \{1,1,...,1\}^{\mathrm{T}},$$
$$\mathbf{u}_B = \{u_B^1, u_B^2, ..., u_B^{N_t}\}^{\mathrm{T}}, \mathbf{w}_B = \{w_B^1, w_B^2, ..., w_B^{N_t}\}^{\mathrm{T}},$$

in which the superscripts indicate the number of time step. From Eq.(53), we have displacements at the free end

$$u_B^k = \sum_{i=1}^{N} A_{Ni} \sin\theta_i(t_k) - 1,\ w_B^k = \sum_{i=1}^{N} A_{Ni} \cos\theta_i(t_k). \tag{62}$$

Integration matrix $\mathbf{A}$ can be obtained by Trapezoidal rule as

$$\mathbf{A}=\begin{pmatrix} 0 & 0 & 0 & 0 & 0 & 0 \\ 1/2 & 1/2 & 0 & 0 & 0 & 0 \\ 1/2 & 1 & 1/2 & 0 & 0 & 0 \\ 1/2 & 1 & 1 & 1/2 & 0 & 0 \\ \cdots & \cdots & \cdots & \cdots & \cdots & \cdots \\ 1/2 & 1 & 1 & 1 & 1 & 1/2 \end{pmatrix}\Delta \tag{63}$$

in which $\Delta = 1/N$. Considering a cantilever uniform cross-section beam with the integration matrix above, we obtain

$$\boldsymbol{\theta}(t_k) = \mathbf{A}\mathbf{h}(t_k) \tag{64}$$

where

$$h_i(t_k) = \frac{L}{EI}\left[F_w^k\left(x_B(t_k) - x_i(t_k)\right) - F_w^k\left(w_B(t_k) - w_i(t_k)\right)\right] \tag{65}$$

In these equations, we have five unknows, i.e. u_B, w_B, θ, F_u and F_w for each time step and that are to be solved from five equations in Eqs (61)(62) and (64). In order to solve this highly non-linear equations, we need to use the iterative technique and the interaction forces F_u^k and F_w^k, for each time step $t_k = k\Delta_t$. Apart from that, we have the following objective

$$R = \text{Minimum}\left\{\left(\sum_j^k a_{kj}F_u^j - 1 + mu_B^k\right)^2 + \left(\sum_j^k a_{kj}F_w^j + mg + mw_B^k\right)^2\right\}. \tag{66}$$

which is equivalent to Eq.(61). Assume that there are no external forces except the constant gravity acting on the concentrated mass, which is suddenly dropped. By using the same iterative algorithm as in the static cases, the dynamic solutions of deflection can be obtained by the following procedure with double loops (*k* for time step and *p* for beam deflection):

Step 1: Set $k = 1$ and specify the interactions $F_u^1 = F_w^1 = 0$;

Step 2: Set $k = k + 1$, time $t = (k-1)\Delta t$, and $F_u^{k+1} = F_u^k$, $F_w^{k+1} = F_w^k$;

Step 3: Set $p = 0$ and specify the initial rotation $\boldsymbol{\theta}(p) = \boldsymbol{\theta}^{(k,p)}$;

Step 4: Calculate vectors $\mathbf{f}_s^{(k,p)}$, $\mathbf{f}_c^{(k,p)}$ and then $\mathbf{h}^{(k,p)}$ from (48)

Step 5: Calculate nodal values of rotations

$$\boldsymbol{\theta}^{(k,p+1)} = \mathbf{A}\mathbf{h}^{(k,p)}; \tag{67}$$

Step 6: Check the relative error of the deflection at the tip, if $\eta < 10^{-5}$ go to Step 9;

Step 7: Introduce the speed up iterative factor λ and modify the deflection for the next iteration

$$\boldsymbol{\theta}^{(k,p+1)} = \lambda \boldsymbol{\theta}^{(k,p)} + (1-\lambda)\boldsymbol{\theta}^{(k,p+1)} \tag{68}$$

Step 8: set $p = p+1$ and go to Step 4;

Step 9: Calculate the objective function R in Eq.(66), if $R < 10^{-5}$, print interaction forces F_u^{k+1}, F_w^{k+1}, displacements u_B^{k+1}, w_B^{k+1}, and if the time incremental step $k = N_t$, computation is terminated;

Step 10: Determine new interaction forces F_u^{k+1}, F_w^{k+1} then go to Step 2;

Consider a uniform cross-section cantilever beam attached with a concentrated mass of *m* at the free end, and the mass is suddenly released and vibration occurs consequently. Uniformly distributed nodes of beam and time axis are considered with $N = 50$ and $N_t = 20$ respectively. Speed factor is $\lambda = 0.8$. The normalized gravity is defined as $\alpha = mgL^2/EI$ and normalized time $\bar{t} = t\sqrt{g/L}$. Figures 19(a) and (b) present the normalized deformations $u_B(t)/L$ and $w_B(t)/L$. In order to illustrate the degree of accuracy, computational results by ABAQUS are shown in Figure 20 when $\alpha = 4$. The difference between these two numerical solutions can be seen in Figure 20. For the material input in ABAQUS, the mass density of the beam has to be specified as a small value rather than zero. In addition, the variations of beam deflection are presented in Figure 21 for different times.

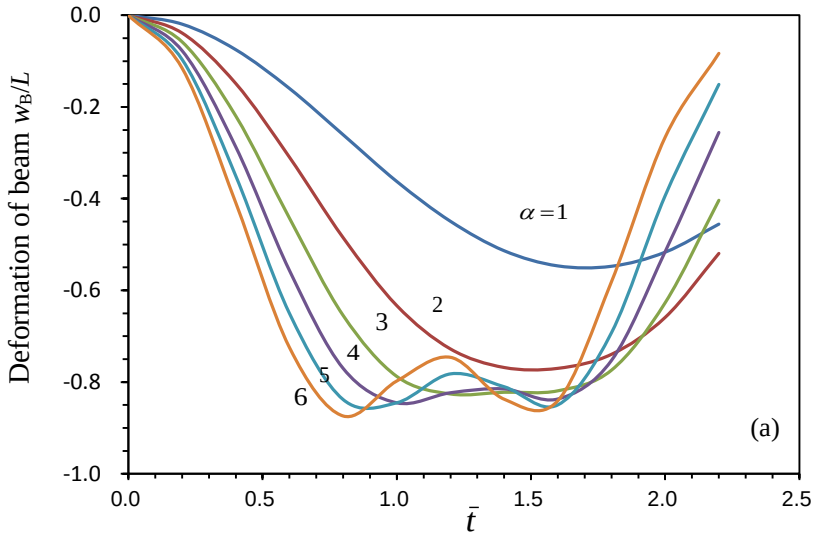

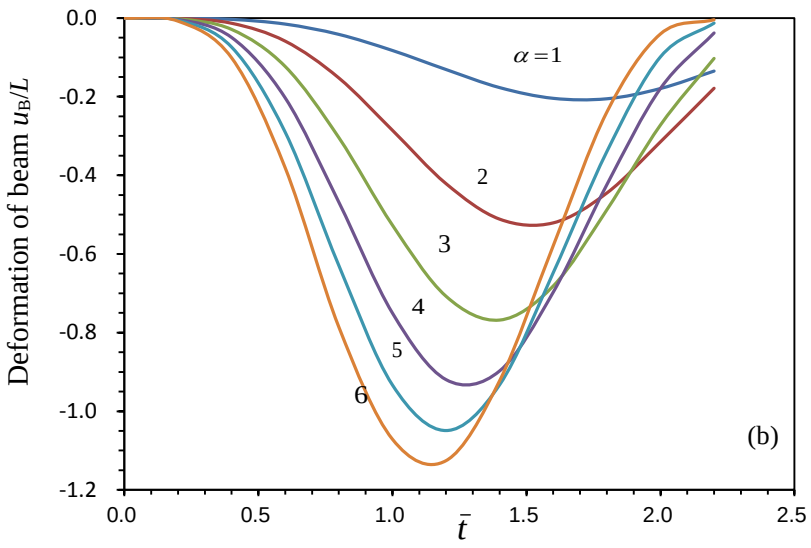

Figure 19. Large deformation of cantilever beam with concentrated mass.

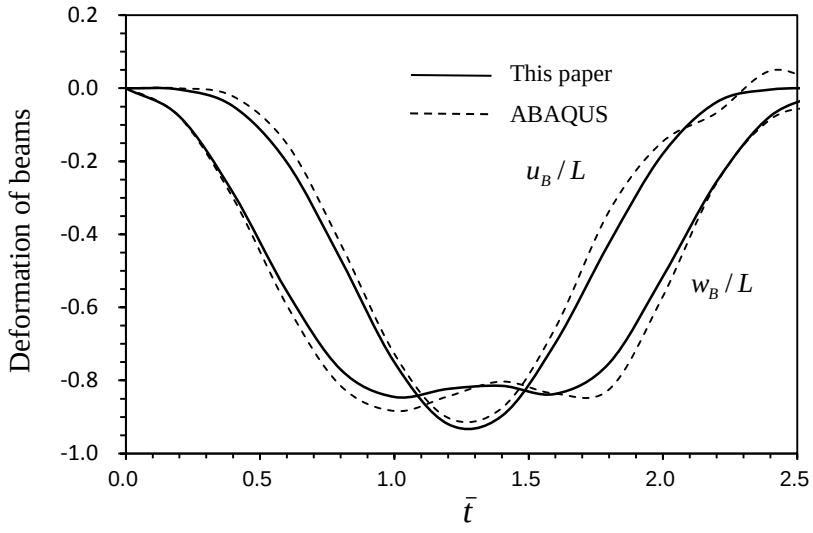

Figure 20. Large deformation of cantilever beam with concentrated mass when $\alpha = 4$.

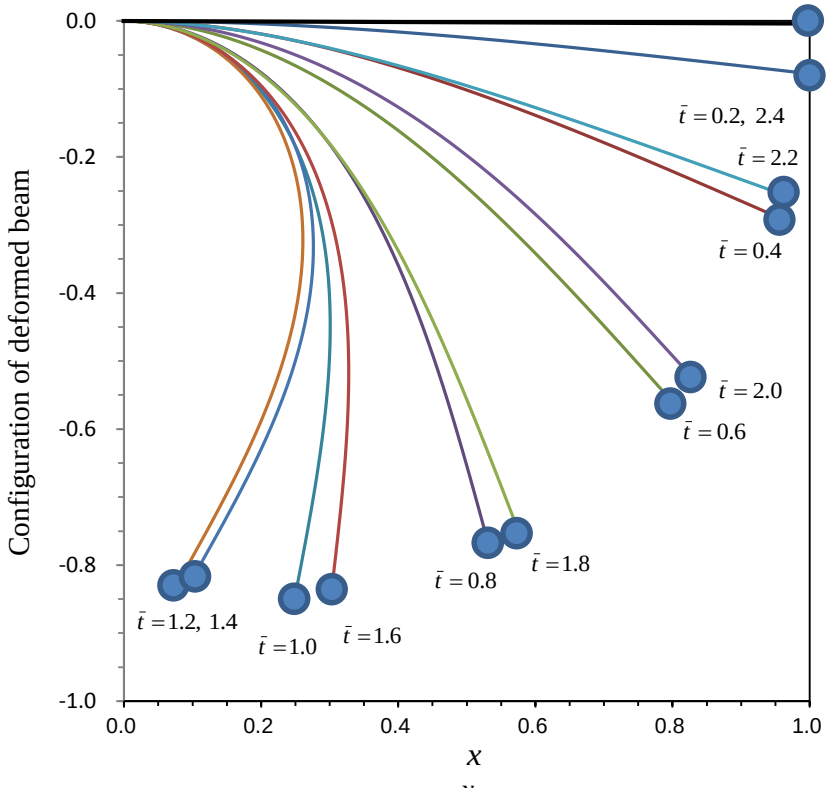

Figure 21. Large deformation of cantilever beam with concentrated mass when $\alpha = 4$..

6. Conclusion

In this paper, large deformation analysis for a cantilever beam with a variable bending stiffness under both static and dynamic loads are investigated by the direct integration scheme. The conclusions are summarized as follows

(1) The solutions of rotation, vertical and horizontal displacements can be obtained without an algebraic equation solver.

(2) The new computational algorithm with its iteration strategy is highly convergent and accurate.

(3) Higher-order equilibrium configurations for a uniform cross-section beam under concentrated follower force can be observed.

(4) There are no second equilibrium configurations for certain tapered beams under a distributed load.

(5) Time dependent solutions of large deformation can be obtained with an integration matrix efficiently.

The presented computational technique can be extended to more complicated problems in engineering including the large deformation analysis of beam of material nonlinearity. There are many complicated cases can be observed including (a) the effect by axial deformation by axial force in the beam, (b) the plasticity of beam under large bending moment and (c) the damping effect caused by the friction force. This will be discussed in a future study.

Acknowledgment.

The first author would like to acknowledge the support of the National Natural Science Foundation of China (51708048).

References

[1] K.E. Bisshop, D.C. Drucker, Large deflection cantilever beams, Q. Appl. Math. 3 (1945) 272–275.

[2] A. Saxena, S.N. Kramer, A simple and accurate method for determining large deflections in compliant mechanisms subjected to end forces and moments, ASME J. Mech. Des. 120 (1998) 392–400.

[3] L.P.Li, K. Schulgasser, G. Cederbaum, Large deflection analysis of poroelastic beams, Int. J. Non-Linear Mechanics, 33(1) (1998) 1-14.

[4] P. Seide, Large deflections of a simply supported beam subjected to moment at one end, J. Appl. Mech. 51 (1984) 519–525.

[5] S. Chucheepsakul, S. Buncharoen, C.M. Wang, Large deflection of beams under moment gradient, J. Eng. Mech. 120 (1994) 1848–1860.

[6] S. Chucheepsakul, S. Buncharoen, T. Huang, Elastica of simple variable-arc-length beam subjected to end moment, J. Eng. Mech. 121 (1995) 767–772.

[7] C.M. Wang, S. Kitipornchai, Shooting optimization technique for large deflection analysis of structural members, Eng. Struct. 14 (1992) 231–240.

[8] C. Kimball, L.-W. Tsai, Modeling of flexural beams subjected to arbitrary end loads, ASME J. Mech. Des. 124 (2002) 223–234.

[9] J. Wang, J-K. Chen, S Liao, An explicit solution of the large deformation of a cantilever beam under point load at the free tip, Journal of Computational and Applied Mathematics 212 (2008) 320 – 330.

[10] X.-F. Li, H. Zhang, K.Y. Lee, Dependence of Young's modulus of nanowires on surface effect, Int. J. Mech. Sci. 81 (2014) 120–125.

[11] X.-L. Peng, X.-F. Li, G.-J. Tang, Z.-B. Shen, Effect of scale parameter on the deflection of a nonlocal beam and application to energy release rate of a crack, Z. Angew. Math. Mech. 95 (2015) 1428–1438.

[12] M. Batista, F. Kosel, Cantilever beam equilibrium configurations, Int. J. Solids and Structures 42(2005) 4663-4672.

[13] M. Batista, Large deflections of a beam subjected to three-point bending, Int. J. Non-Linear Mechanics 69 (2015) 84-92.

[14] J. Argyris, Sp Symeonidis, Nonlinear finite element analysis of elastic systems under nonconservative loading-natural formulation. Part 1. Quasistatic problems, Computer Methods in Applied Mechanics and Engineering 26 (1981) 75–123.

[15] B.S. Shvartsman, Large deflections of a cantilever beam subjected to a follower force, J Sound and Vibration 304 (2007) 969–973.

[16] R.D. Wood, O.C. Zienkiewicz, Geometrically nonlinear finite element analysis of beams, frames, arches and axisymmetric shells, Comput. Struct. 7 (1977) 725–735.

[17] G. Baker, On the large deflections of non-prismatic cantilevers with a finite depth, Comput. Struct. 46 (1993) 365–370.

[18] B.K. Lee, J.F. Wilson, S.J. Oh, Elastica of cantilevered beams with variable cross section, Int. J. Non-linear Mech. 28 (1993) 579–589.

[19] D,K. Nguyen, S.G. Buntara, Large deflections of tapered functionally graded beams subjected to end forces, Applied Mathematical Modelling 38 (2014) 3054–3066

[20] A. Banerjee, B. Bhattacharya, A.K. Mallik, Large deflection of cantilever beams with geometric non-linearity: Analytical and numerical approaches, Int. J. Nonlin. Mech. 43 (2008) 366-376.

[21] M. Saje, Finite element formulation of finite planar deformation of curved elastic beams, Comput. Struct. 39 (1991) 327-337.

[22] B.N. Rao, G.V. Rao, On the large deflection of cantilever beams with end rotational load, Zeitschrift fur Angewandte Mathematik und Mechanik 66(1986) 507-508.

[23] B.N. Rao, B.P. Shastry, G.V. Rao, Large deflections of a cantilever beam subjected to a tip concentrated rotational load, Aeronautical Journal 90(1986) 262-266.

[24] B.N. Rao, G.V. Rao, Large deflections of a non-uniform cantilever beam with end rotational load, Forschung Ingenieurwesen 54 (1988) 24-26

[25] P.H. Wen, Y.C. Hon, M. Li, T. Korakianitis, Finite integration method for partial differential equations, Appl Math Model 37(24)(2013) 10092–106.

[26] M. Li, Y.C. Hon, T. Korakianitis, P.H. Wen, Finite integration method for nonlocal elastic bar under static and dynamic loads, Eng Anal Bound Elem 37(5)(2013) 842–9.

[27] M. Li, C.S. Chen, Y.C. Hon, P.H. Wen, Finite integration method for solving multi-dimensional partial differential equations, Appl Math Model 39(17)(2015) 4979–94.

[28] D.L. Yun, Z.I. Wen, Y.C. Hon, Adaptive least squares finite integration method for higher- dimensional singular perturbation problems with multiple boundary layers, Appl Math Comput. 271(2015) 232–50.

[29] Y. Li, M. Li, Y.C. Hon, Improved finite integration method for multi-dimensional nonlinear burgers' equation with shock wave, Neural Parallel Sci. Comput. 23(2015) 63–86.

[30] Y. Li, Y.C. Hon, Finite integration method with radial basis function for solving stiff problems, Eng Anal Bound Elem 107(2019) 115–123.

[31] T. Huang, Y. Yuan, J.L. Zheng, E. Avital, P.H. Wen, Large deformations of tapered beam with finite integration method, Eng Anal Bound Elem 82(2017) 32–42.

[32] M. Mutyalarao, D. Bharathi, B. N. Rao, On the uniqueness of large deflections of a uniform cantilever beam under a tip-concentrated rotational load, Int. J. Non-Linear Mechanics 45 (2010) 433-441.

[33] M. Batista, Discussion of 'On the uniqueness of large deflections of a uniform cantilever beam under a tip-concentrated rotational load' by M. Mutyalarao, D. Bharathi, B. N. Rao, Int. J. Non-Linear Mechanics 54 (2013) 127-130.

Responses to reviews' comments

Dear Reviewer

I would like to thank you very much for reviewing our work carefully and providing comments in order to improve the quality of manuscript. You are comments have been addressed in the revised version. Few amendments are marked in Red.

Best regards

Dr P.H. Wen on behalf all authors of the manuscript.

Reviewer #2: This manuscript presents an extension of authors' previous works [25] to large-deformation beam analysis. The described technique for solving numerically large-deformation analysis of cantilever beam is novel and is a meaningful contribution to the development of finite integration method (FIM). This strategy appears very promising in terms of mathematical simplicity, computational efficiency and easy programming. The organization of this paper is logical and easy to follow, numerical results are solid and the interpretation of results is adequate.

Overall, this is a well-written paper on a subject that could be of much interest to researchers using the FIM for nonlinear analysis, especially for nonlinear beam analysis, as is the application here. I recommend the editor to accept this paper with Mathematics and Computers in Simulation after some minor revisions as detailed below.

1. The reviewer understands that the authors plan to look at more challenging problems in the future. Therefore, in the end of the paper, the authors may give some comments on the problems that are actually studied or will be studied in the future.

Response: Thanks reviewer's positive comments for our paper. The future research work following sentences are added:

"There are many complicated cases can be observed including (a) the effect by axial deformation by axial force in the beam, (b) the plasticity of beam under large bending moment and (c) the damping effect caused by the friction force."

2. I think that it would be useful to give the readers the flowchart of the whole numerical procedure, including generation of points, etc.

Response: Thanks for reviewer pointing out this issue. The numerical details with flowchart are added in the revised version marked in the red as below

In addition, the computation procedure is demonstrated in the flowchart in Figure 10.

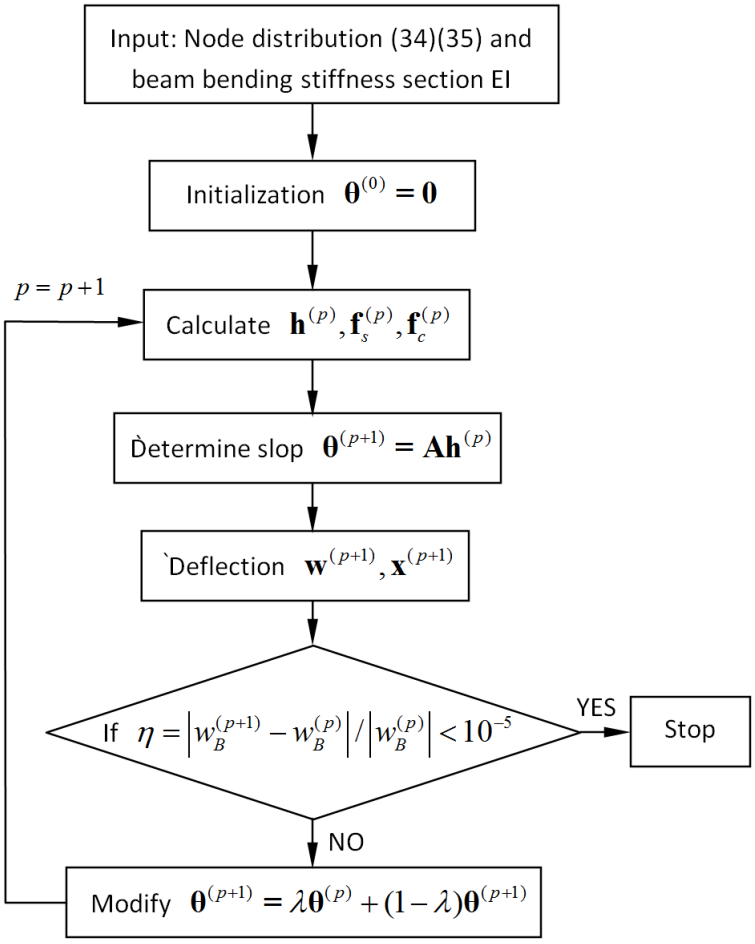

Figure 10. Computation iterative steps for nonlinear problem.